

AnySat: An Earth Observation Model for Any Resolutions, Scales, and Modalities

Guillaume Astruc^{1,3,4}Nicolas Gonthier^{1,2}Clement Mallet¹Loic Landrieu^{1,4}¹ LASTIG, Univ Gustave Eiffel, IGN, ENSG, France² IGN, France³ CNES, France⁴ LIGM, Ecole Nationale des Ponts et Chaussées, IP Paris, Univ Gustave Eiffel, CNRS, France

Abstract

Geospatial models must adapt to the diversity of Earth observation data in terms of resolutions, scales, and modalities. However, existing approaches expect fixed input configurations, which limits their practical applicability. We propose AnySat, a multimodal model based on joint embedding predictive architecture (JEPA) and scale-adaptive spatial encoders, allowing us to train a single model on highly heterogeneous data in a self-supervised manner. To demonstrate the advantages of this unified approach, we compile GeoPlex, a collection of 5 multimodal datasets with varying characteristics and 11 distinct sensors. We then train a single powerful model on these diverse datasets simultaneously. Once fine-tuned, we achieve better or near state-of-the-art results on the datasets of GeoPlex and 4 additional ones for 5 environment monitoring tasks: land cover mapping, tree species identification, crop type classification, change detection, and flood segmentation. The code and models are available at <https://github.com/gastruc/AnySat>.

1. Introduction

From a remote sensing perspective, the natural images of computer vision are remarkably uniform: they are captured by nearly identical sensors (standard cameras) with the same RGB channels and are often taken from similar perspectives. This consistency allows the creation of large composite image datasets from various sources [25, 52, 59], which are key for image foundation models to learn powerful, general-purpose features [8].

In contrast, Earth observation (EO) data displays significant variability in modalities, scales, and spatial, temporal, and spectral resolutions. Existing EO foundation models are generally trained on a single dataset with a specific format [11, 32, 44, 71], and cannot be applied to datasets with different input types without retraining from scratch—defeating the purpose of foundation models. EO foundation models should be able to seamlessly integrate new datasets for training and prediction, regardless of their resolution, scale,

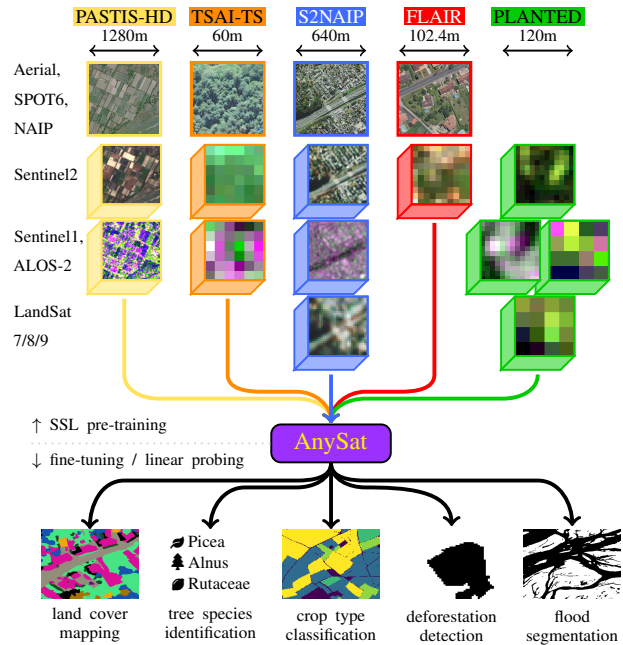


Figure 1. **Multi-Dataset Training.** For the first time, a single model can be pretrained **simultaneously** on a collection of Earth Observation datasets with heterogeneous resolutions, scales, and modalities. The resulting model can be fine-tuned to achieve state-of-the-art results for a wide variety of data types and tasks.

and modalities. As recent efforts provide more flexibility in terms of modalities [7, 39], scale [54], or spectral resolutions [75], none fully leverage the diversity of EO sensors.

We introduce **AnySat**, a novel EO model using the spatial alignment of multiple modalities as a source of self-supervision. Indeed, while multiple observations of the same area from distinct sensors capture different information, they share the same underlying semantics. Therefore, we can expect the learned representations to be consistent across modalities. Moreover, we should be able to reconstruct missing modalities from available ones, encouraging the use of cross-modal masked auto-encoding techniques [7, 35]. However, EO data are subject to complex disruptors such as

weather conditions, acquisition angles, and variations in time of day or year. To overcome this issue, we design a new multimodal Joint Embedding Predictive Architecture (JEPA) [6] to learn representations that are consistent *in feature space*.

A key advantage of our JEPA model is that it eliminates the need for modality-specific decoders, allowing us to handle a wide variety of sensors seamlessly. Combined with our scale-adaptive patch encoders, this approach enables us to train a single model on highly heterogeneous collections of multimodal EO datasets. Notably, over 75% of the learnable parameters in our model are shared across all modalities and resolutions, and thus benefit from a large and varied source of data for self-supervision.

To evaluate our approach, we compile **GeoPlex**, a collection of 5 multimodal datasets including 11 distinct modalities, with aerial images and satellite time series, radar and optical sensors. GeoPlex spans various spatial resolutions (from 0.2 to 250 m per pixel), revisit times (from single images to weekly time series), channel counts (3 to 11), and spatial extent (samples ranging from 0.4 to 160 hectares). To showcase the versatility of AnySat, we also consider 4 external evaluation datasets with diverse characteristics. After fine-tuning, AnySat achieves state-of-the-art performance on 7 downstream tasks, including classification, segmentation, and change segmentation across domains such as land cover mapping, crop type classification, tree species identification, and deforestation detection. Our contributions are as follows:

- We present AnySat, a versatile architecture capable of learning from multiple EO sources with heterogeneous resolutions, scales, and modalities.
- We introduce the first application of JEPA for multimodal EO data, enabling large-scale and efficient self-supervised learning.
- We demonstrate that, when pretrained on a curated collection of EO datasets, AnySat can be fine-tuned to achieve state-of-the-art performance across a diverse array of tasks and datasets.

Thanks to its versatility, our powerful pretrained model can be applied to a wide variety of applications and datasets—from unimodal data to any combination of the 11 sensors featured in GeoPlex, and scales from single forest plots to large urban areas spanning several hectares.

2. Related Work

In this section, we review the dynamic field of self-supervised learning in geospatial models, highlighting recent efforts to enhance their adaptability to diverse inputs. Finally, we present the feature-predictive paradigm, which is instrumental to improve the versatility of EO models.

Self-Supervised Geospatial Models. The abundance of raw EO data makes it particularly suitable for self-supervised

learning approaches [9, 14, 46, 67]. Generative models leverage the unique properties of EO data with adapted strategies such as spectral [19], temporal [22, 23], and spatio-temporal [39, 77], and hybrid [66] masking. Other approaches predict rotated [42] or rescaled [49, 54, 63] versions of the input data, or predict missing modalities from available ones [7, 24]. However, these models are often trained on specific combinations of modalities and are limited to those modalities during inference, which hinders their applicability as foundation models expected to adapt to diverse scenarios.

Versatile EO Models. Several approaches have been proposed to improve the generalizability of EO models. Some models address variability in spatial resolutions by training on images of different resolutions and generalizing to coarser scales [54], while others manage spectral variability by training on sensors with different spectral bands [75]. Temporal adaptability is achieved in models capable of handling both single-date images and image time series [7, 11, 32]. Attempts have also been made to generalize across modalities by training on data from different sensors [37, 39] or and even text or audio [58]. Despite these efforts, many models are still trained with a single scale and expect the input to have a certain shape, typically 224×224 pixels. They resize other inputs to fit the model architecture, leading to inefficiencies for smaller inputs [66, Tab 5]. A key obstacle preventing the creation of truly versatile generative self-supervised models is the requirement for multiple encoders, decoders, and augmentations to handle different configurations. In this paper, we explore feature-predictive architectures as a promising solution to this challenge.

Feature-Predictive Architectures. Self-supervised learning methods have achieved significant success in image analysis [17, 34, 52]. These approaches learn without labels using pretext tasks, which can be discriminative [30, 50], contrastive [16, 17, 31, 34], or generative, where the model predicts a degraded version of its input [35, 70]. Recent works have proposed performing reconstruction in feature space rather than input space (*e.g.*, pixel space) [10, 76]. Among feature-predictive architectures, the Joint Embedding Predictive Architecture (JEPA) has shown particular promise [6] by learning to predict the features of masked parts of an input image. Feature space reconstruction based model can also be combined with contrastive objectives for improved stability and representation quality [10].

Because it bypasses the need for complex data augmentations or decoder networks, JEPA is particularly well-suited for massively multimodal applications such as Earth observation. SAR-JEPA [41] introduces the first implementation of JEPA concepts for EO, focusing exclusively on SAR data. In this paper, we combine JEPA with a versatile spatial encoder architecture, allowing a single model to handle diverse data

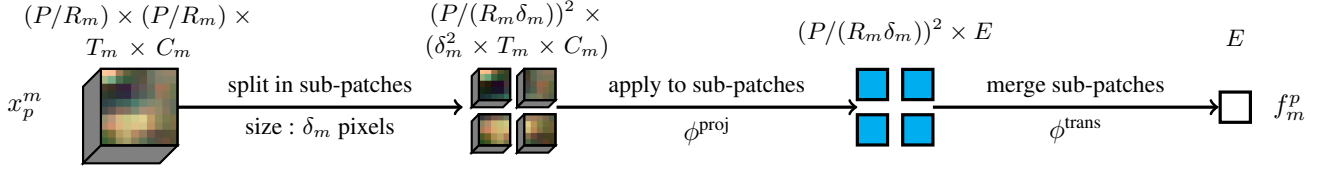


Figure 2. **Scale-Adaptive Patch Encoding.** We propose an architecture that can encode patches of different sizes. We consider a patch x_p^m of size P (in m) and resolution R_m (in m). We first split x_p^m into sub-patches of size δ_m pixels, which are processed by a modality-specific projector ϕ_m^{proj} . Then, a shared transformer module ϕ^{trans} combines the sub-patches into a vector of size E . The sub-patch size δ_m is fixed, and only influences the number of input tokens to ϕ^{trans} , allowing us to use the same configuration for different patch sizes P .

scales, resolutions, and modalities.

3. Method

We first detail our proposed architecture (Sec. 3.1) and self-supervised training procedure (Sec. 3.2). We then explain how to fine-tune the model for downstream tasks (Sec. 3.3). A key motivation of this work is multi-dataset self-supervised training. For simplicity, we first explain how our model operates with a single multimodal dataset and then generalize it to multiple datasets.

3.1. Architecture

Our model processes multimodal tiles by first partitioning them into spatially aligned patches. Unlike classical Vision Transformers [21], our model can handle patches of different sizes, allowing us to adapt to the significant scale variations in EO datasets. Each patch is embedded using a scale-adaptive patch encoder, and a combiner network merges the representations from multiple modalities into a unified representation for each spatial patch.

We consider a tile x of size $S \times S$ meters observed through a set of modalities \mathbf{M} . Each modality $m \in \mathbf{M}$ is characterized by its resolution R_m (size of a pixel in meters), the number of temporal observations T_m (with $T_m = 1$ for single-date modalities), and the number of channels C_m (e.g., spectral channels or polarization ratios). We denote by x^m the observation of tile x in modality m , represented as a tensor of size $(S/R_m) \times (S/R_m) \times T_m \times C_m$.

Spatially Consistent Patching. We divide the tile x into a set \mathbf{P} of non-overlapping patches of size $P \times P$ meters. For each patch $p \in \mathbf{P}$ and modality $m \in \mathbf{M}$, we define an input token x_p^m , which corresponds to the observation of patch p in modality m . This results in $(S/P)^2$ tokens per modality and a total of $|\mathbf{M}| \cdot (S/P)^2$ tokens. Since the patch size P is consistent across all modalities, all input tokens $\{x_p^m\}_{m \in \mathbf{M}}$ correspond to the same spatial region. However, the dimensions of each token x_p^m —given by $(P/R_m) \times (P/R_m) \times T_m \times C_m$ —may vary between modalities due to differences in spatial, temporal, and spectral resolutions.

Patch Encoding. Handling datasets with tiles of varying extents requires adapting our patch size: the 6×6 Sentinel-2 tiles of TreeSatAI [3] can be processed with 1×1 patches, but this would be impractical for the 128×128 Sentinel-2 tiles of the PASTIS dataset [28]. We propose a patch encoder ϕ^{patch} that embeds each patch x_p^m into a fixed-size vector f_p^m of dimension E , regardless of its resolution R_m and size P .

As our patches can have varying temporal dimensions and spatial extents that can reach hundreds of pixels, we do not use FlexiVit’s [12] weight rescaling. In the spirit of the Perceiver [38], we adopt instead a 2 stage embedding scheme. We first divide each token x_p^m into sub-patches of fixed size δ_m pixels, resulting in $(P/(R_m \delta_m))^2$ sub-patches per token. Each sub-patch has dimensions $\delta_m \times \delta_m \times T_m \times C_m$.

As illustrated in Fig. 2, we map each sub-patch to dimension E with the function ϕ_m^{proj} , defined as follows:

- (i) If $T_m > 1$, we apply to each pixel a Lightweight Temporal Attention Encoder (LTAE) $\phi_m^{\text{temp}} : T_m \times C_m \mapsto E$ [27] to collapse the temporal dimension. If $T = 1$, we use a linear layer $C_m \mapsto E$.
- (ii) We flatten the pixel dimensions of each sub-patch to obtain a vector of size $\delta_m^2 E$;
- (iii) We apply a Multi-Layer Perceptron (MLP) $\delta_m^2 E \mapsto E$ to each sub-patch;
- (iv) We add absolute positional encodings based on the ground sampling distance, as in ScaleMAE [54];
- (v) A shared transformer network ϕ^{trans} with B blocks combines the sub-patches into a single vector f_p^m of size E with a CLS-like token.

The patch encoder ϕ^{patch} thus consists of $|\mathbf{M}|$ modality-specific projectors ϕ_m^{proj} and a shared transformer ϕ^{trans} for all modalities. Using sub-patches of fixed sizes δ_m allows ϕ^{patch} to process patches of different patch sizes P without rescaling the input data. Indeed, changes in P only influence the number of input token processed by ϕ^{trans} , which has no incidence on the size of the class token.

Modality-Combiner Network. We merge the embeddings f_p^m for tokens of different modalities into a single multimodal vector f_p^* for each patch. We first add to each f_p^m an absolute positional encoding $\text{pos}(p)$ (the same one used for

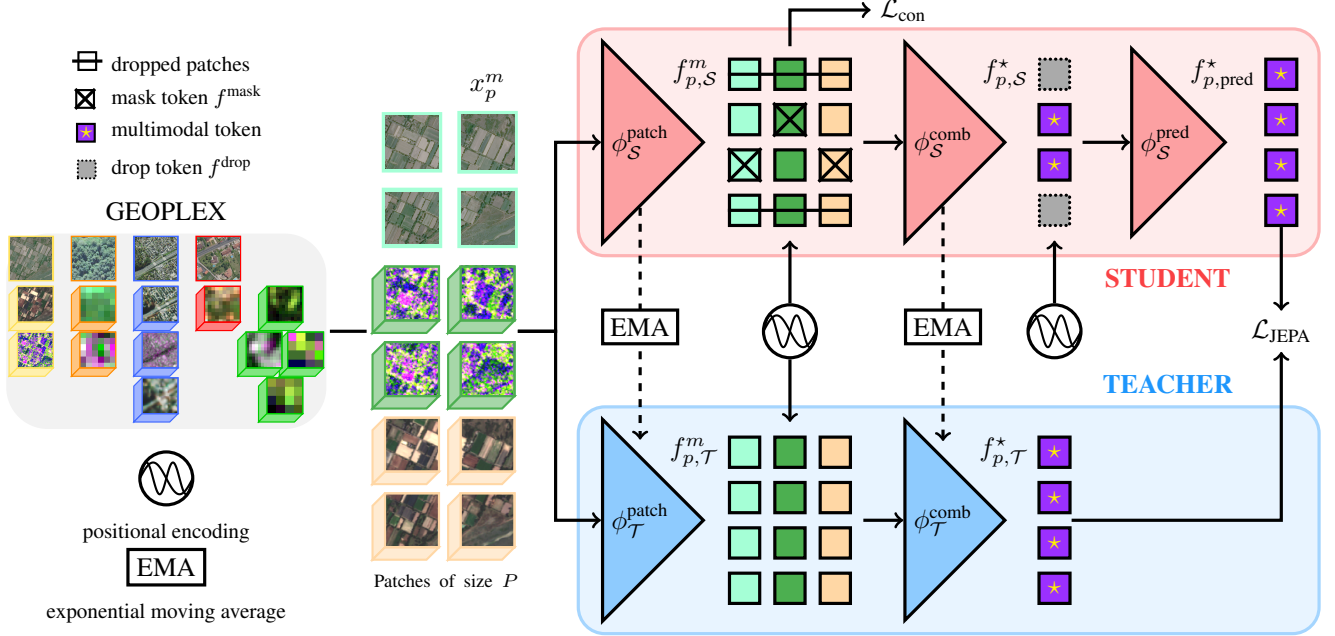


Figure 3. **Architecture of AnySat.** We begin each iteration by randomly selecting a dataset among GeoPlex and sampling a tile. Each available modality is divided into spatially aligned patches of size P . The student network’s patch encoder ϕ_S^{patch} embeds each patch and we apply a contrastive loss to encourage spatial consistency across modalities. We then apply dropping and masking : some patches have all modalities removed (dropping), while others have only random modalities removed (masking). The remaining patches are merged in the modality combiner ϕ_S^{comb} to form multimodal representations f_S^* for the non-dropped patches. The predictor ϕ_S^{pred} then reconstructs the embeddings of the dropped patches. Finally, the student network’s output is compared to the teacher’s, whose weights are an Exponential Moving Average (EMA) of the student’s weights and which processes the complete set of patches without masking or dropping.

sub-patches). The combiner network ϕ^{comb} summarizes the resulting token embeddings into a multimodal representation f_p^* for each patch $p \in \mathbf{P}$. The combiner network follows the architecture proposed by OmniSat [7, 3.1]: (i) The tokens go through a sequence of B self-attention blocks; (ii) We add one token per patch, with a fixed (and learned) value and add positional encoding; and (iii) We compute the cross-attention between these tokens and the embeddings of the last self-attention block. The resulting values (one per patch) define multimodal embeddings f_p^* .

3.2. Training

We adapt the Joint Embedding Predictive Architecture (JEPA) framework [6] to multimodal EO, allowing AnySat to be pretrained in a self-supervised manner on datasets with varying properties and modalities, without labels. The general idea is that a student network operates on heavily masked inputs— spatially, temporally, and modality-wise— while the teacher network sees all the input information. The student’s goal is to combine all its available information to predict the teacher’s embeddings. We combine this model with a contrastive loss for improved stability.

Student-Teacher Architecture. We consider two versions of the network: a *student* and a *teacher*. The student network consists of a patch encoder ϕ_S^{patch} , a modality combiner ϕ_S^{comb} , and a predictor network ϕ_S^{pred} . The teacher network includes a patch encoder ϕ_T^{patch} and a modality combiner ϕ_T^{comb} . The weights of the teacher network are updated as an Exponential Moving Average (EMA) of the student’s weights [34]. The student’s predictor network ϕ_S^{pred} is composed of a residual positional encoding and three residual self-attention blocks, and the teacher does not have a predictor.

The student network embeds all input tokens x_p^m into vectors of size E using the patch encoder:

$$f_{p,S}^m = \phi_S^{\text{patch}}(x_p^m). \quad (1)$$

We now present the two loss functions used to train the student model: a contrastive loss and a JEPA loss.

Contrastive Loss. For a fixed patch p , the observations x_p^m for $m \in \mathcal{M}$ capture different aspects of the same spatial region but share the same underlying semantics: the content of p . Therefore, we expect the representations $f_{p,S}^m$ to be consistent across modalities.

We enforce this intuition with a contrastive loss inspired by OmniSat [7]. Specifically, we use a modified InfoNCE

loss [51], where each token (p, m) is positively matched with tokens of the same patch but different modalities, and negatively matched with tokens corresponding to different patches and modalities. Tokens of the same modality but different patches are neither counted as positive nor negative, as patches of the same tile can have similar content. The contrastive loss is defined as:

$$\mathcal{L}_{\text{con}} = \sum_{(p,m) \in \mathbf{P} \times \mathbf{M}} \frac{-\log}{|\mathbf{P}| |\mathbf{M}|} \left(\frac{\sum_{n \neq m} \exp(\langle f_{p,S}^m, f_{p,S}^n \rangle / \tau)}{\sum_{\substack{n \neq m \\ q \neq p}} \exp(\langle f_{p,S}^m, f_{q,S}^n \rangle / \tau)} \right), \quad (2)$$

where τ is a temperature parameter, and $\langle \cdot, \cdot \rangle$ denotes the cosine similarity between embeddings.

Joint Embedding Predictive Architecture. We adapt the JEPA self-supervised learning framework [6] to the context of multimodal Earth Observation. Avoiding reconstruction in pixel space is particularly beneficial for EO data, which can be heavily influenced by factors such as weather, time of day, or acquisition angle. Reconstructing in latent space allows us to learn more consistent and semantically meaningful features. The training process proceeds as follows:

- **Patch Dropping.** We apply JEPA’s multi-block masking strategy by randomly selecting five rectangular regions on the tile. Let $\mathbf{K} \subset \mathbf{P}$ be the set of patches intersected by these rectangles, and $\bar{\mathbf{K}} = \mathbf{P} \setminus \mathbf{K}$ the remaining patches. We drop all the student’s tokens $f_{p,S}^m$ for patches $p \in \mathbf{K}$.
- **Modality & Temporal Masking:** We randomly mask a subset $\mathbf{L} \subset \bar{\mathbf{K}} \times \mathbf{M}$ of the remaining tokens, ensuring that at least one modality per patch remains unmasked. Masked token embeddings are replaced with a fixed value $f^{\text{mask}} \in \mathbb{R}^E$, which is learned as a parameter of the network. We also randomly mask 50% of the timestamps of all time series.
- **Combiner:** We add positional encodings to all tokens and input them to the student’s combiner ϕ_S^{comb} , producing multimodal embeddings $f_{p,S}^*$ for $p \in \bar{\mathbf{K}}$:

$$f_{p,S}^* = \phi_S^{\text{comb}}(\{f_{p,S}^m\}_{(p,m) \notin \mathbf{L}} \cup \{f^{\text{mask}}\}_{(p,m) \in \mathbf{L}}). \quad (3)$$

- **Predictor:** We replace each dropped patch $p \in \mathbf{K}$ with a fixed value $f^{\text{drop}} \in \mathbb{R}^E$. We add positional encodings to all tokens (including the dropped ones) and input them to the predictor ϕ_S^{pred} , yielding embeddings $f_{p,\text{pred}}^*$ for all patches $p \in \mathbf{P}$:

$$f_{p,\text{pred}}^* = \phi_S^{\text{pred}}(\{f_{p,S}^*\}_{p \in \bar{\mathbf{K}}} \cup \{f^{\text{drop}}\}_{p \in \mathbf{K}}). \quad (4)$$

- **Teacher Encoding:** The teacher network receives all input tokens x_p^m , embeds them using $\phi_{\mathcal{T}}^{\text{patch}}$, and combines

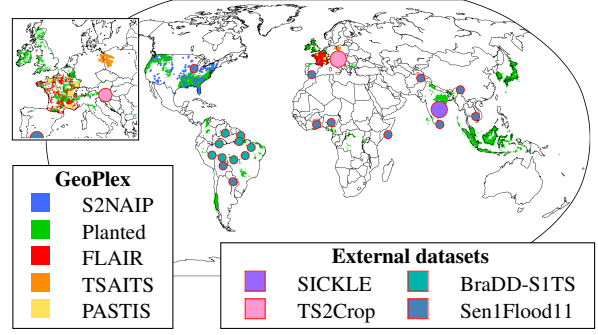


Figure 4. **Datasets Considered.** GeoPlex is composed of 5 diverse dataset spanning the entire world, with a higher concentration in Europe and the US where open-data are more abundant. We also consider external evaluation datasets with a more diverse spread.

them with $\phi_{\mathcal{T}}^{\text{comb}}$ without any dropping, masking, or temporal dropout. The teacher outputs patch embeddings $f_{p,\mathcal{T}}^*$ for all $p \in \mathbf{P}$.

- **Loss Function:** The training objective is the L_2 distance between the student predictions and the teacher’s multimodal embeddings for the dropped patches:

$$\mathcal{L}_{\text{JEPA}} = \frac{1}{|\mathbf{K}|} \sum_{p \in \mathbf{K}} \|f_{p,\text{pred}}^* - f_{p,\mathcal{T}}^*\|_2^2. \quad (5)$$

After training, we use the teacher network for downstream tasks and discard the student. Note that all modules are shared across all modalities except for the projection layers ϕ_m^{proj} in the patch encoder ϕ^{patch} .

Training with Multiple Datasets. The flexibility of AnySat enables us to train a single model simultaneously on several datasets of various sizes and scales with the same weights and without rescaling. We consider a set \mathbf{D} of such datasets. Each dataset $d \in \mathbf{D}$ is characterized by the subset $M_d \subset \mathbf{M}$ of its available modalities and S_d the size of its tiles. We also consider a batch size B_d and a set P_d of acceptable patch sizes, which depend on the nature of the data, the available resolution, and the tile size. We use the following procedure:

1. Randomly select a dataset d in \mathbf{D} .
2. Randomly select a patch size P in P_d .
3. Randomly sample B_d tiles in d .
4. Process the tiles and backpropagate the loss.

3.3. Downstream Tasks

After pretraining our model, we fine-tune it for various downstream tasks such as classification, semantic segmentation, and panoptic segmentation.

Classification. In this task, we predict a label or set of labels for each tile. We add a [CLS] token in the cross-

Test sets of datasets from GeoPlex

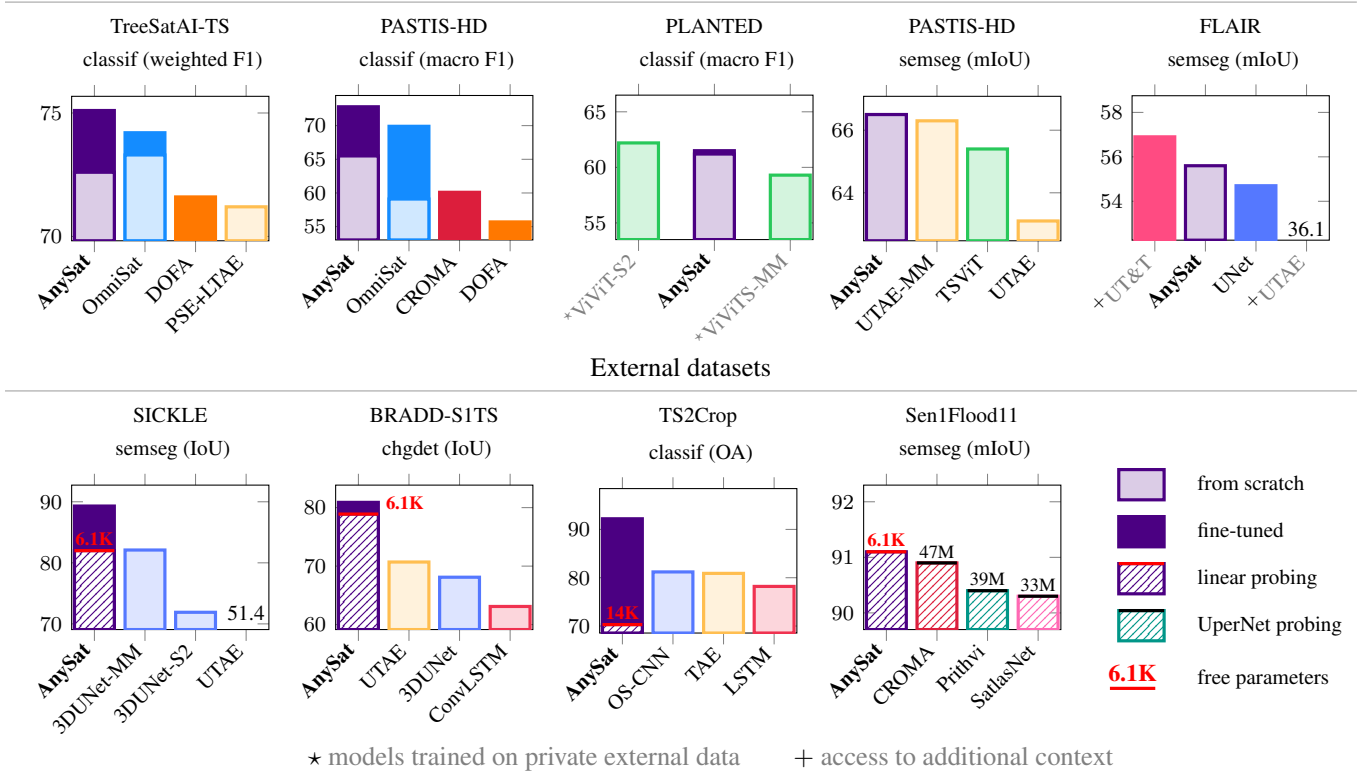


Figure 5. **Quantitative Evaluation.** We evaluate AnySat across 9 open-access datasets and for four tasks: multilabel classification (classif), semantic segmentation (semseg), pixel-wise change detection (chgdet), and pixel-wise regression (regression). For clarity, we only visualize the four best performance per plot. We report the number of trainable parameters for probing evaluation with a frozen network.

attention module of the combiner network, allowing it to output a tile-wise representation alongside the multimodal patch tokens. A linear layer then maps this representation to a vector of logits corresponding to the classification labels.

Semantic Segmentation. Here, we predict a label for each pixel at a specific spatial resolution. We first select a modality m , usually one with a resolution close to that of the annotations. We create a feature map at the subpatch resolution δ_m by concatenating the subpatch embeddings (output of ϕ_m^{proj}) with the multimodal embedding of their corresponding patch (output of ϕ^{comb}). An MLP is then applied to each subpatch to map the concatenated to a vector of logits of size $\delta_m \times \delta_m \times N$, where N is the number of semantic classes. We reshape—and, if necessary, resample using bilinear interpolation—to obtain a map of pixel logits at the label resolution. Note that this approach allows us to perform linear probing for segmentation, without having to use a complex segmentation head such as UPerNet [74], as is usually done in this setting [47].

4. Experiments

4.1. Datasets and Evaluation

We present the datasets used for training and evaluation, as well as our evaluation protocol.

GeoPlex. As argued by Roscher *et al.* [56], EO models benefit from high-quality, diverse, and curated data rather than extensive but uniform acquisitions. We follow this intuition by compiling a collection of five multimodal datasets, each featuring different combinations of modalities, scales, and resolutions. Unless specified otherwise, GeoPlex comprises the training sets of the following datasets:

- **TreeSatAI-TS** [3, 7]: A forest-centric dataset in Germany with Sentinel-1 & 2 time series and Very High Resolution (VHR) images at 0.2 m resolution.
- **FLAIR** [26]: A French land cover dataset with Sentinel-2 time series and VHR images with elevation data (0.2 m). In order to form multimodal patches, we crop the Sentinel-2 time series to match the extent of the VHR images (discarding 93.5% of pixels).
- **PLANTED** [53]: A global forest dataset comprising time series from multiple sensors, including Sentinel-

1/2, Landsat-7, ALOS-2, and MODIS. Only 1.3 of the 2.3M images used in the paper are publicly available.

- **S2NAIP-URBAN** [11]: An urban dataset in the continental US with VHR images (1.25m) and time series from Sentinel-1/2 and Landsat-8/9.
- **PASTIS-HD** [7, 28]: A French crop mapping dataset with VHR images (1.5m) and Sentinel-1 & 2 time series. As PASTIS is evaluated in 5-fold cross-validation, there are no dedicated train and test sets. We include the entire dataset (without labels) in GeoPlex.

As illustrated in Fig. 4, GeoPlex spans 249K km² across five continents and 171 billion pixels. The sampled tiles range in size from 0.36 to 164 hectares. GeoPlex includes 11 distinct modalities with resolutions ranging from 0.2 m to 250 m, with both VHR images and time series data:

- **Very High Resolution Images:**
 - **Aerial:** RGB+NIR (near-infrared) at 0.2 m
 - **Aerial+NMS:** RGB+NIR+Elevation at 0.2 m
 - **NAIP:** RGB+NIR at 1.25 m
 - **SPOT6:** RGB+NIR at 1.5 m.
- **Time Series Data:**
 - **Sentinel-1:** 3 channels (VV/VH polarization + ratio) at 10 m, Ascending & Descending Orbits
 - **Sentinel-2:** 10 channels at 10 m
 - **ALOS-2:** 3 channels (polarization) at 30 m
 - **Landsat-7:** 6 channels at 30 m
 - **Landsat-8/9:** 11 channels at 30 m
 - **MODIS:** 7 channels at 250 m.

We select the possible patch size per dataset, while we set the sub-patch size per modality 1 pixel for very high-resolution images and 10 pixels for time series data. See the Appendix for the complete characteristics of all datasets. The official repository contains scripts to compile GeoPlex and add new datasets.

External Datasets. To showcase AnySat’s flexibility, we also consider 4 datasets not included in GeoPlex. AnySat can be directly fine-tuned or linearly probed on new datasets, even if their exact modality combination is not featured in GeoPlex. We consider the following datasets:

- **SICKLE** [57]: A multimodal crop mapping dataset in India featuring Sentinel-1, Sentinel-2, and Landsat-8 time series. As the test set has not been released, we use the validation set.
- **BraDD-S1TS** [40]: A change detection dataset comprising Sentinel-1 time series of the Amazon rainforest, aiming to segment deforested areas.
- **TimeSen2Crop** [72]: A crop mapping dataset in Slovenia consisting of *single-pixel* Sentinel-2 time series, a modality not present in GeoPlex.
- **Sen11Flood1** [13]: A global flood mapping dataset with

Table 1. **External Datasets.** We evaluate our pretrained model on 4 external datasets, in the fine-tuning or linear probing settings. 🗄️ stands for single-date observations. We report the number of trainable parameters for probing experiments.

SICKLE [57]	L8	S1	S2	mIoU
AnySat (fine-tune)	✓	✓	✓	89.3
AnySat (linear 6.1K)	✓	✓	✓	82.0
Unet3d [45, 57]	✓	✓	✓	82.1
UTAE [28, 57]	✓	✓	✓	51.4
BraDD-S1TS [40]		S1		mIoU
AnySat (fine-tune)		✓		80.9
AnySat (linear 6.1K)		✓		78.9
UTAE [28]		✓		70.7
3D-UNet [45]		✓		68.1
Conv-LSTM [61]		✓		63.7
TimeSen2Crop [72]			S2	OA
AnySat (fine-tune)			✓	92.2
AnySat (linear 14K)			✓	70.3
OS-CNN [64, 70]			✓	81.2
MLP+TAE [27, 69]			✓	80.9
W.LSTM [15, 60]			✓	78.2
Transformer [68]			✓	78.1
MSResNet [20]			✓	76.3
Sen1Floods11 [13]		S1	S2	mIoU
AnySat (linear 6.1K)		🗄️	🗄️	91.1
CROMA [24] (UperNet 47M)		🗄️	🗄️	90.9
Prithvi [39] (UperNet 39M)		🗄️	🗄️	90.4
SatlasNet [11] (UperNet 33M)		🗄️	🗄️	90.3

pixel annotations and single-date Sentinel-1 and 2 observations, a modality not present in GeoPlex. Each tile covers 2600 hectares.

Note that SICKLE’s LandSat8 requires 3 bands not present in S2NAIP’s LandSat8. Conversely, TimeSen2Crop only provide 9 of the 10 bands used to train our Sentinel-2 projector network. In all cases, we use our pretrained projectors and pad the missing channels with a learned value shared across all datasets, sensors, and channels.

Evaluation. We evaluate our model on the annotated datasets of GeoPlex (excluding S2NAIP-URBAN) and the 4 external datasets, across three tasks: (i) **Classification:** TSAIT-TS, PASTIS-HD, PLANTED, TimseSenCrop; (ii) **Semantic Segmentation:** PASTIS-HD, FLAIR, SICKLE, Sen1Flood11; and (iii) **Binary pixel-wise change detection:** BraDD-S1TS.

We use three evaluation setting to evaluate the models:

- **From Scratch.** The model is trained directly on the labeled training set in a supervised manner.
- **Fine-tuning.** The model is pretrained in a self-supervised manner, then fine-tuned on the training set.
- **Linear Probing.** The model is initially pretrained in a self-supervised manner, and a linear layer is fitted with the training set. This experiment is reserved for external datasets.

Note that most foundation models pretrained on external data cannot be directly applied to target datasets with different input configurations. For example, the ScaleMAE and SatMAE models trained on the Functional Map of the World [18] and are limited to RGB bands, while CROMA is trained on single-date Sentinel-2 data. Since these specific modalities are not present in any of our evaluation datasets, we cannot directly evaluate these pretrained models. Instead, we modify the input layers of these models to match the target number of spectral bands and pre-train them from scratch on each training set separately.

Competing Methods. We compare AnySat against state-of-the-art Earth Observation models. Since most models are not designed to handle multimodal or multitemporal inputs, we adapt them following the protocol established by Astruc *et al.* [7]: (i) we set up independent copies of the model process each modality, followed by a feature fusion scheme; (ii) time series are converted into single images either by concatenating seasonal medians or selecting a pre-determined date, depending on which yields the best results; and (iii) smaller backbones (*e.g.*, ViT-L to ViT-S) are used when they improve performance on smaller datasets.

We report for Sen1flood11 the performance of models trained with a frozen encoder and a fine-tuned UperNet [74] as given by the PANGAEA benchmark [48]. In contrast, AnySat can be linearly probed for semantic segmentation, which requires up 7,000 times fewer free parameters.

4.2. Results and Analysis

We evaluate our model on different datasets from and outside of GeoPlex with fine-tuning and linear probing.

Performance on GeoPlex’ Test Sets. We evaluate AnySat on the test sets of the GeoPlex datasets, as shown in Fig. 5, with detailed results provided in the Appendix. Despite using a single pretrained model, AnySat sets new state-of-the-art results for TreeSatAI-TS (+0.9 weighted F1 score) and PASTIS-HD (+2.8 mIoU in classification and +0.2 in segmentation). AnySat also achieves near state-of-the-art performance on PLANTED [53], even though the ViViT models [5] were trained on a withheld dataset with nearly 80% more data of the same type. Similarly, our model performs close to the state-of-the-art on FLAIR, despite

having access to only 6.5% of the extent of the Sentinel-2 tiles used by UT&T [26].

Pretraining on GeoPlex consistently improves performance, indicating that training on a collection of datasets with varied modalities leads to richer and more robust representations. The improvement is more pronounced for smaller datasets like TreeSatAI-TS and in classification tasks rather than segmentation. We attribute this to the amount of supervision available in larger datasets and dense annotations, which make pretraining less beneficial.

Performance on External Datasets. As shown in Tab. 1, AnySat pretrained on GeoPlex significantly surpasses the state-of-the-art on the three external datasets: +3.6 mIoU for SICKLE, +10.2% mIoU for BraDD-S1TS, and +11.0 OA for TimeSen2Crop. This shows the strong generalization capabilities of our model despite differences in sensor configurations, such as missing channels. Moreover, while GeoPlex mostly spans the northern hemisphere, SICKLE and BraDDS1TS are in India and Brazil, respectively.

Furthermore, AnySat is the first EO model that can be effectively linearly probed for semantic segmentation and achieves competitive results. Indeed, AnySat outperforms all dedicated approaches on BraDD-S1TS with linear probing. Moreover, AnySat achieve in linear probing better performance on Sen1flood11 than foundation models which fine-tuned UperNet segmentation heads, with up to 7000 times more free parameters. These results highlight the expressiveness of the features learned through our self-supervised training scheme. Our pretrained AnySat model can thus be adapted to new tasks and data with minimal training cost and yield competitive results.

Ablation Study. We evaluate the impact of several key design choices and report the results in Tab. 2. All results are presented for the Fold 5 of PASTIS-HD and for the classification and semantic segmentation tasks. We do not pretrain on the entire GeoPlex but use Fold 1 to 4 of PASTIS-HD in a self-supervised fashion.

- **Random Token Dropping.** We replaced JEPA’s block masking strategy with purely random token dropping for the student network. This modification decreased classification performance but slightly improved segmentation results. In order to use a single model configuration for all tasks, we maintained a unified approach. Interestingly, block masking does not appear to be as critical for EO data than for natural images (see Table 6 in [6]).
- **No Contrastive Loss.** We remove the contrastive loss and retain only the reconstruction loss $\mathcal{L}_{\text{JEPA}}$. This substantially reduces the classification performance (−4.3 F1) but only a moderate decrease in segmentation performance (−0.2 mIoU). These findings suggest that the contrastive loss can help the feature-predictive approach

Table 2. **Ablation.** We evaluate the impact for several critical design choices of our model on the Fold 1 of PASTIS-HD.

Experiment	classification macro F1	segmentation mIoU
best configuration	72.0	63.6
random token dropping	71.3	64.1
no contrastive	67.7	63.4
naive semseg	-	61.2

learn more discriminative features, particularly benefiting classification tasks.

- **Naive Semantic Segmentation.** We predict pixel-wise logits directly from the patch embeddings without utilizing subpatch features. This results in a decrease in segmentation performance by 2.4 mIoU, highlighting the importance of subpatches in providing fine-grained spatial information.

Inference and Training Times. Our model was pretrained on GeoPlex using 1760 GPU-hours on an NVIDIA H100 GPU. Fine-tuning takes between 10 and 40 hours, depending on the dataset size. Linear probing takes approximately 2 hours on BraDD-SITS.

In terms of inference speed, AnySat processes one monochrome tile from TreeSatAI [3] in 3ms on average, which is faster than ScaleMAE [54] (10ms) and comparable to DOFA [75] (3ms) and OmniSat [7] (2ms).

5. Conclusion

We have presented AnySat, a versatile architecture designed to address the diversity of EO data in terms of resolutions, scales, and modalities. By leveraging a joint embedding predictive architecture and scale-adaptive spatial encoders, AnySat can be trained in a self-supervised manner on highly heterogeneous datasets. Pretrained on GeoPlex, a comprehensive collection of multimodal datasets with varying characteristics, our model achieved state-of-the-art performance across multiple datasets, tasks, and modalities.

A key advantage of AnySat is its ability to be applied and fine-tuned on a wide array of combinations of data types and scales with a single model. Moreover, new datasets can be easily incorporated into GeoPlex for self-supervised pre-training. Our goal is to generalize this approach to develop a versatile foundation model for environmental monitoring on a global scale.

Acknowledgement

This work was granted access to the HPC resources of IDRIS under the allocations AD011014719 and AD011014286R1 made by GENCI. We thank Jordi Inglada, Antoine Labatie,

Dimitris Samaras, Yohann Perron, Vincent Lepetit for inspiring discussions and valuable feedback.

References

- [1] Lightning: LinearWarmupCosineAnnealingLR. <https://lightning-flash.readthedocs.io/en/stable/api/generated/flash.core.optimizers.LinearWarmupCosineAnnealingLR.html>. Accessed: 2024-11-20. 17
- [2] PyTorch: ReduceLROnPlateau. [org/docs/stable/generated/torch.optim.lr_scheduler.ReduceLROnPlateau.html#torch.optim.lr_scheduler.ReduceLROnPlateau](https://pytorch.org/docs/stable/generated/torch.optim.lr_scheduler.ReduceLROnPlateau.html#torch.optim.lr_scheduler.ReduceLROnPlateau). Accessed: 2024-02-29. 17
- [3] Steve Ahlswede, Christian Schulz, Christiano Gava, Patrick Helber, Benjamin Bischke, Michael Förster, Florencia Arias, Jörn Hees, Begüm Demir, and Birgit Kleinschmit. TreeSatAI Benchmark Archive: A multi-sensor, multi-label dataset for tree species classification in remote sensing. *Earth System Science Data Discussions*, 2022. 3, 6, 9, 16, 17
- [4] allenai.org. AI2-S2-NAIP. <https://huggingface.co/datasets/allenai/s2-naip>, 2024. [Online; accessed 01-Sept-2024]. 16, 17
- [5] Anurag Arnab, Mostafa Dehghani, Georg Heigold, Chen Sun, Mario Lučić, and Cordelia Schmid. ViViT: A video vision transformer. In *CVPR*, 2021. 8, 15
- [6] Mahmoud Assran, Quentin Duval, Ishan Misra, Piotr Bojanowski, Pascal Vincent, Michael Rabbat, Yann Lecun, and Nicolas Ballas. Self-supervised learning from images with a joint-embedding predictive architecture. In *CVPR*, 2023. 2, 4, 5, 8
- [7] Guillaume Astruc, Nicolas Gonthier, Clement Mallet, and Loic Landrieu. Omnisat: Self-supervised modality fusion for earth observation. In *ECCV*, 2024. 1, 2, 4, 6, 7, 8, 9, 14, 15, 16, 17
- [8] Muhammad Awais, Muzammal Naseer, Salman Khan, Rao Muhammad Anwer, Hisham Cholakkal, Mubarak Shah, Ming-Hsuan Yang, and Fahad Shahbaz Khan. Foundational models defining a new era in vision: A survey and outlook. *arXiv preprint arXiv:2307.13721*, 2023. 1
- [9] Kumar Ayush, Burak Uzkent, Chenlin Meng, Kumar Tanmay, Marshall Burke, David Lobell, and Stefano Ermon. Geography-aware self-supervised learning. In *ICCV*, 2021. 2
- [10] Alexei Baevski, Wei-Ning Hsu, Qiantong Xu, Arun Babu, Jiatao Gu, and Michael Auli. Data2vec: A general framework for self-supervised learning in speech, vision and language. In *ICML*, 2022. 2, 15

- [11] Favyen Bastani, Piper Wolters, Ritwik Gupta, Joe Ferdinando, and Aniruddha Kembhavi. SatlasPretrain: A large-scale dataset for remote sensing image understanding. In *ICCV*, 2023. 1, 2, 7
- [12] Lucas Beyer, Pavel Izmailov, Alexander Kolesnikov, Mathilde Caron, Simon Kornblith, Xiaohua Zhai, Matthias Minderer, Michael Tschannen, Ibrahim Alabdulmohsin, and Filip Pavetic. Flexivit: One model for all patch sizes. In *CVPR*, 2023. 3
- [13] Derrick Bonafilia, Beth Tellman, Tyler Anderson, and Erica Issenberg. Sen1Floods11: A georeferenced dataset to train and test deep learning flood algorithms for Sentinel-1. In *CVPR Workshop EarthVision*, 2020. 7, 14, 16, 18
- [14] Jules Bourcier, Gohar Dashyan, Karteek Alahari, and Jocelyn Chanussot. Learning representations of satellite images from metadata supervision. In *ECCV*, 2024. 2
- [15] Lorenzo Bruzzone and Sebastiano B Serpico. Classification of imbalanced remote-sensing data by neural networks. *Pattern recognition letters*, 1997. 7
- [16] Mathilde Caron, Hugo Touvron, Ishan Misra, Hervé Jégou, Julien Mairal, Piotr Bojanowski, and Armand Joulin. Emerging properties in self-supervised vision transformers. In *ICCV*, 2021. 2
- [17] Ting Chen, Simon Kornblith, Mohammad Norouzi, and Geoffrey Hinton. A simple framework for contrastive learning of visual representations. In *ICML*, 2020. 2
- [18] Gordon Christie, Neil Fendley, James Wilson, and Ryan Mukherjee. Functional map of the world. In *CVPR*, 2018. 8
- [19] Yezhen Cong, Samar Khanna, Chenlin Meng, Patrick Liu, Erik Rozi, Yutong He, Marshall Burke, David Lobell, and Stefano Ermon. SatMAE: Pre-training transformers for temporal and multi-spectral satellite imagery. In *NeurIPS*, 2022. 2, 15
- [20] Bo Dang and Yansheng Li. MSResNet: Multiscale residual network via self-supervised learning for waterbody detection in remote sensing imagery. *Remote Sensing*, 2021. 7
- [21] Alexey Dosovitskiy, Lucas Beyer, Alexander Kolesnikov, Dirk Weissenborn, Xiaohua Zhai, Thomas Unterthiner, Mostafa Dehghani, Matthias Minderer, Georg Heigold, Sylvain Gelly, et al. An image is worth 16x16 words: Transformers for image recognition at scale. In *ICLR*, 2020. 3
- [22] Iris Dumeur, Silvia Valero, and Jordi Inglada. Paving the way toward foundation models for irregular and unaligned satellite image time series. *arXiv preprint arXiv:2407.08448*, 2024. 2
- [23] Iris Dumeur, Silvia Valero, and Jordi Inglada. Self-supervised spatio-temporal representation learning of satellite image time series. *IEEE Journal of Selected Topics in Applied Earth Observations and Remote Sensing*, 2024. 2
- [24] Anthony Fuller, Koreen Millard, and James R Green. CROMA: Remote sensing representations with contrastive radar-optical masked autoencoders. In *NeurIPS*, 2023. 2, 7, 15
- [25] Samir Yitzhak Gadre, Gabriel Ilharco, Alex Fang, Jonathan Hayase, Georgios Smyrnis, Thao Nguyen, Ryan Marten, Mitchell Wortsman, Dhruva Ghosh, Jieyu Zhang, et al. Datacomp: In search of the next generation of multimodal datasets. In *NeurIPS*, 2024. 1
- [26] Anatol Garioud, Nicolas Gonthier, Loic Landrieu, Apolline De Wit, Marion Valette, Marc Poupée, Sébastien Giordano, and Boris Watrelos. FLAIR: A country-scale land cover semantic segmentation dataset from multi-source optical imagery. In *NeurIPS Dataset and Benchmark*, 2023. 6, 8, 14, 15, 16, 17
- [27] Vivien Sainte Fare Garnot and Loic Landrieu. Lightweight temporal self-attention for classifying satellite images time series. In *Advanced Analytics and Learning on Temporal Data: ECML PKDD Workshop*, 2020. 3, 7, 15
- [28] Vivien Sainte Fare Garnot and Loic Landrieu. Panoptic segmentation of satellite image time series with convolutional temporal attention networks. In *ICCV*, 2021. 3, 7, 14, 15, 16
- [29] Vivien Sainte Fare Garnot, Loic Landrieu, and Nesrine Chehata. Multi-modal temporal attention models for crop mapping from satellite time series. *ISPRS Journal of Photogrammetry and Remote Sensing*, 2022. 15, 17
- [30] Spyros Gidaris, Praveer Singh, and Nikos Komodakis. Unsupervised representation learning by predicting image rotations. In *ICLR*, 2018. 2
- [31] Jean-Bastien Grill, Florian Strub, Florent Altché, Corentin Tallec, Pierre Richemond, Elena Buchatskaya, Carl Doersch, Bernardo Avila Pires, Zhaohan Guo, Mohammad Gheshlaghi Azar, et al. Bootstrap your own latent—a new approach to self-supervised learning. In *NeurIPS*, 2020. 2
- [32] Xin Guo, Jiangwei Lao, Bo Dang, Yingying Zhang, Lei Yu, Lixiang Ru, Liheng Zhong, Ziyuan Huang, Kang Wu, Dingxiang Hu, et al. Skysense: A multi-modal remote sensing foundation model towards universal interpretation for earth observation imagery. In *CVPR*, 2024. 1, 2, 15
- [33] Kaiming He, Xiangyu Zhang, Shaoqing Ren, and Jian Sun. Deep residual learning for image recognition. In *CVPR*, 2016. 15
- [34] Kaiming He, Haoqi Fan, Yuxin Wu, Saining Xie, and Ross Girshick. Momentum contrast for unsupervised visual representation learning. In *CVPR*, 2020. 2, 4, 15

- [35] Kaiming He, Xinlei Chen, Saining Xie, Yanghao Li, Piotr Dollár, and Ross Girshick. Masked autoencoders are scalable vision learners. In *CVPR*, 2022. 1, 2
- [36] Danfeng Hong, Bing Zhang, Xuyang Li, Yuxuan Li, Chenyu Li, Jing Yao, Pedram Ghamisi, Naoto Yokoya, Hao Li, Xiuping Jia, Antonio Plaza, Paolo Gamba, Jon Atli Benediktsson, and Jocelyn Chanussot. SpectralGPT: Spectral remote sensing foundation model. *TPAMI*, 2024. 15
- [37] Chia-Yu Hsu, Wenwen Li, and Sizhe Wang. Geospatial foundation models for image analysis: Evaluating and enhancing NASA-IBM Prithvi’s domain adaptability. *International Journal of Geographical Information Science*, 2024. 2
- [38] Andrew Jaegle, Felix Gimeno, Andy Brock, Oriol Vinyals, Andrew Zisserman, and Joao Carreira. Perceiver: General perception with iterative attention. In *ICML*. PMLR, 2021. 3
- [39] Johannes Jakubik, S Roy, CE Phillips, P Fraccaro, D Godwin, B Zadrozny, D Szwarcman, C Gomes, G Nyirjesy, B Edwards, et al. Foundation models for generalist geospatial artificial intelligence. URL <https://arxiv.org/abs/2310.18660>. 1, 2, 7, 15
- [40] Kaan Karaman, V Sainte Fare Garnot, and Jan Dirk Wegner. Deforestation detection in the Amazon with Sentinel-1 SAR image time series. *ISPRS Annals of the Photogrammetry, Remote Sensing and Spatial Information Sciences*, 2023. 7, 14, 16, 17
- [41] Weijie Li, Wei Yang, Tianpeng Liu, Yuenan Hou, Yuxuan Li, Zhen Liu, Yongxiang Liu, and Li Liu. Predicting gradient is better: Exploring self-supervised learning for sar atr with a joint-embedding predictive architecture. *ISPRS Journal of Photogrammetry and Remote Sensing*, 2024. 2
- [42] Zhihao Li, Biao Hou, Siteng Ma, Zitong Wu, Xianpeng Guo, Bo Ren, and Licheng Jiao. Masked angle-aware autoencoder for remote sensing images. *arXiv preprint arXiv:2408.01946*, 2024. 2
- [43] Ilya Loshchilov and Frank Hutter. Decoupled weight decay regularization. In *ICLR*. 17
- [44] Siqi Lu, Junlin Guo, James R Zimmer-Dauphinee, Jordan M Nieusma, Xiao Wang, Parker VanValkenburgh, Steven A Wernke, and Yuankai Huo. AI foundation models in remote sensing: A survey. *arXiv preprint arXiv:2408.03464*, 2024. 1
- [45] Rose M Rustowicz, Robin Cheong, Lijing Wang, Stefano Ermon, Marshall Burke, and David Lobell. Semantic segmentation of crop type in Africa: A novel dataset and analysis of deep learning methods. In *CVPR Workshop EarthVision*, 2019. 7
- [46] Oscar Manas, Alexandre Lacoste, Xavier Giró-i Nieto, David Vazquez, and Pau Rodriguez. Seasonal contrast: Unsupervised pre-training from uncurated remote sensing data. In *ICCV*, 2021. 2
- [47] Valerio Marsocci and Nicolas Audebert. Cross-sensor self-supervised training and alignment for remote sensing. *arXiv preprint arXiv:2405.09922*, 2024. 6
- [48] Valerio Marsocci, Yuru Jia, Georges Le Bellier, David Kerekes, Liang Zeng, Sebastian Hafner, Sebastian Gerard, Eric Brune, Ritu Yadav, Ali Shibli, et al. PANGAEA: A global and inclusive benchmark for geospatial foundation models. *arXiv preprint arXiv:2412.04204*, 2024. 8
- [49] Mubashir Noman, Muzammal Naseer, Hisham Cholakkal, Rao Muhammad Anwer, Salman Khan, and Fahad Shahbaz Khan. Rethinking transformers pre-training for multi-spectral satellite imagery. In *CVPR*, 2024. 2
- [50] Mehdi Noroozi and Paolo Favaro. Unsupervised learning of visual representations by solving jigsaw puzzles. In *ECCV*, 2016. 2
- [51] Aaron van den Oord, Yazhe Li, and Oriol Vinyals. Representation learning with contrastive predictive coding. *arXiv preprint arXiv:1807.03748*, 2018. 5
- [52] Maxime Oquab, Timothée Darcet, Théo Moutakanni, Huy Vo, Marc Szafraniec, Vasil Khalidov, Pierre Fernandez, Daniel Haziza, Francisco Massa, Alaaeldin El-Nouby, et al. Dinov2: Learning robust visual features without supervision. *TLMR*, 2023. 1, 2, 15
- [53] Luis Miguel Pazos-Outón, Cristina Nader Vasconcelos, Anton Raichuk, Anurag Arnab, Dan Morris, and Maxim Neumann. Planted: A dataset for planted forest identification from multi-satellite time series. *International Geoscience and Remote Sensing Symposium*, 2024. 6, 8, 15, 16, 17
- [54] Colorado J Reed, Ritwik Gupta, Shufan Li, Sarah Brockman, Christopher Funk, Brian Clipp, Kurt Keutzer, Salvatore Candido, Matt Uyttendaele, and Trevor Darrell. Scale-MAE: A scale-aware masked autoencoder for multiscale geospatial representation learning. In *ICCV*, 2023. 1, 2, 3, 9, 15, 17
- [55] Esther Rolf, Jonathan Proctor, Tamma Carleton, Ian Bolliger, Vaishaal Shankar, Miyabi Ishihara, Benjamin Recht, and Solomon Hsiang. A generalizable and accessible approach to machine learning with global satellite imagery. *Nature communications*, 2021. 15
- [56] Ribana Roscher, Marc Russwurm, Caroline Gevaert, Michael Kampffmeyer, Jefersson A. Dos Santos, Maria Vakalopoulou, Ronny Hänsch, Stine Hansen, Keiller Nogueira, Jonathan Prexl, and Devis Tuia. Better, not just more: Data-centric machine learning for Earth observation. *IEEE Geoscience and Remote Sensing Magazine*, 2024. 6
- [57] Depanshu Sani, Sandeep Mahato, Sourabh Saini, Harsh Kumar Agarwal, Charu Chandra Devshali, Saket

- Anand, Gaurav Arora, and Thiagarajan Jayaraman. SICKLE: A multi-sensor satellite imagery dataset annotated with multiple key cropping parameters. In *WACV*, 2024. 7, 14, 16, 18
- [58] Srikumar Sastry, Subash Khanal, Aayush Dhakal, Adeel Ahmad, and Nathan Jacobs. TaxaBind: A unified embedding space for ecological applications. In *WACV*, 2025. 2
- [59] Christoph Schuhmann, Romain Beaumont, Richard Vencu, Cade Gordon, Ross Wightman, Mehdi Cherti, Theo Coombes, Aarush Katta, Clayton Mullis, Mitchell Wortsman, et al. Laion-5b: An open large-scale dataset for training next generation image-text models. In *NeurIPS Dataset and benchmark*, 2022. 1
- [60] Hochreiter Sepp and Schmidhuber Jürgen. Long short-term memory. *Supervised sequence labelling with recurrent neural networks*, 2012. 7
- [61] Xingjian Shi, Zhourong Chen, Hao Wang, Dit-Yan Yeung, Wai-Kin Wong, and Wang-Chun Woo. Convolutional LSTM network: A machine learning approach for precipitation nowcasting. In *NeurIPS*, 2015. 7
- [62] Adam Stewart, Nils Lehmann, Isaac Corley, Yi Wang, Yi-Chia Chang, Nassim Ait Ali Braham, Shradha Sehgal, Caleb Robinson, and Arindam Banerjee. SSSL4EO-I: Datasets and foundation models for Landsat imagery. *NeurIPS*, 36, 2024. 15
- [63] Maofeng Tang, Andrei Cozma, Konstantinos Georgiou, and Hairong Qi. Cross-scale mae: A tale of multiscale exploitation in remote sensing. In *NeurIPS*, 2024. 2
- [64] Wensi Tang, Guodong Long, Lu Liu, Tianyi Zhou, Michael Blumenstein, and Jing Jiang. Omni-scale CNNs: A simple and effective kernel size configuration for time series classification. In *ICLR*, 2021. 7
- [65] Michail Tarasiou, Erik Chavez, and Stefanos Zafeiriou. ViTs for SITS: Vision transformers for satellite image time series. In *CVPR*, 2023. 15
- [66] Gabriel Tseng, Ivan Zvonkov, Mirali Purohit, David Rolnick, and Hannah Kerner. Lightweight, pre-trained transformers for remote sensing timeseries. *arXiv preprint arXiv:2304.14065*, 2023. 2, 15
- [67] Wei-Hsin Tseng, Hoàng-Ân Lê, Alexandre Boulch, Sébastien Lefèvre, and Dirk Tiede. CROCO: Cross-modal contrastive learning for localization of Earth observation data. *ISPRS Annals of the Photogrammetry, Remote Sensing and Spatial Information Sciences*, 2022. 2
- [68] Ashish Vaswani, Noam Shazeer, Niki Parmar, Jakob Uszkoreit, Llion Jones, Aidan N Gomez, Łukasz Kaiser, and Illia Polosukhin. Attention is all you need. In *NeurIPS*, 2017. 7
- [69] Elliot Vincent, Jean Ponce, and Mathieu Aubry. Satellite image time series semantic change detection: Novel architecture and analysis of domain shift. *arXiv preprint arXiv:2407.07616*, 2024. 7
- [70] Pascal Vincent, Hugo Larochelle, Yoshua Bengio, and Pierre-Antoine Manzagol. Extracting and composing robust features with denoising autoencoders. In *ICML*, 2008. 2, 7
- [71] Yi Wang, Nassim Ait Ali Braham, Zhitong Xiong, Chenying Liu, Conrad M Albrecht, and Xiao Xiang Zhu. SSL4EO-S12: A large-scale multi-modal, multi-temporal dataset for self-supervised learning in Earth observation. *IEEE Geoscience and Remote Sensing Magazine*, 2023. 1
- [72] Giulio Weikmann, Claudia Paris, and Lorenzo Bruzzone. Timesen2crop: A million labeled samples dataset of Sentinel 2 image time series for crop-type classification. *IEEE Journal of Selected Topics in Applied Earth Observations and Remote Sensing*, 2021. 7, 16, 18
- [73] Piper Wolters, Favyen Bastani, and Aniruddha Kembhavi. Zooming out on zooming in: Advancing super-resolution for remote sensing, 2023. 16, 17
- [74] Tete Xiao, Yingcheng Liu, Bolei Zhou, Yuning Jiang, and Jian Sun. Unified perceptual parsing for scene understanding. In *ECCV*, 2018. 6, 8
- [75] Zhitong Xiong, Yi Wang, Fahong Zhang, Adam J Stewart, Joëlle Hanna, Damian Borth, Ioannis Papoutsis, Bertrand Le Saux, Gustau Camps-Valls, and Xiao Xiang Zhu. Neural plasticity-inspired foundation model for observing the Earth crossing modalities. *arXiv preprint arXiv:2403.15356*, 2024. 1, 2, 9, 15
- [76] Kun Yi, Yixiao Ge, Xiaotong Li, Shusheng Yang, Dian Li, Jianping Wu, Ying Shan, and Xiaohu Qie. Masked image modeling with denoising contrast. In *ICLR*, 2023. 2
- [77] Yuan Yuan, Lei Lin, Qingshan Liu, Renlong Hang, and Zeng-Guang Zhou. SITS-Former: A pre-trained spatio-spectral-temporal representation model for sentinel-2 time series classification. *International Journal of Applied Earth Observation and Geoinformation*, 2022. 2

AnySat: An Earth Observation Model for Any Resolutions, Scales, and Modalities

Supplementary Material

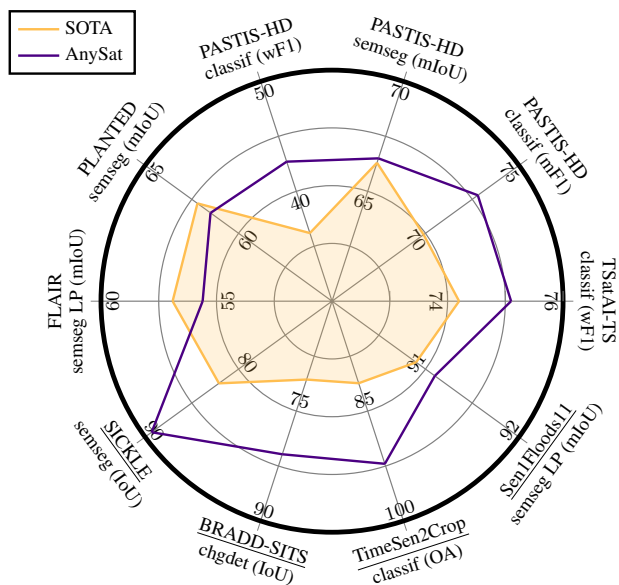


Figure A. **Overall Performance.** We underline external datasets. LP stands for Linear Probing.

In this appendix, we provide detailed results in Sec. A, an extended ablation study in Sec. B, and provide implementation details in Sec. C. Finally, we provide more details on the datasets and experiments of the main paper in Sec. D

A. Detailed Results

We provide qualitative illustrations of our predictions and detailed quantitative results for the test sets of GeoPlex.

Qualitative Results. We present qualitative illustrations in Fig. B for four segmentation tasks: PASTIS, FLAIR, SICKLE, and BraDD-SITS. AnySat predicts precise segmentations that closely follow the extents of buildings, trees, and parcels. Notably, the predictions do not display grid artifacts despite our segmentation head being a simple linear layer applied to each subpatch. This suggests that using subpatches of small sizes (*e.g.*, 4×4 pixels for PASTIS and 10×10 pixels for FLAIR), combined with larger context through patch embeddings, is an effective strategy for producing smooth and consistent segmentation maps.

Quantitative Results. We provide in Tab. A the detailed performance of AnySat, with and without pretraining, and an extensive comparison with recent EO models. Pretraining on GeoPlex improves performance for smaller datasets (*e.g.*,

TreeSatAI-TS, PASTIS in classification), but this effect is more limited for segmentation datasets (FLAIR, PASTIS in segmentation) or larger ones like PLANTED. We hypothesize that this is due to the quantity of available supervision; for instance, FLAIR has over 20 billion individual labels. In the case of FLAIR, the pretrained model is 0.5 points behind training from scratch, which we attribute to stochastic noise, as our performance on the validation set is on par with training from scratch: 54.7 for pretrained vs. 54.8 from scratch.

B. Additional Ablation

We propose an additional experiment to evaluate the impact of one of our design choices.

No Modality or Temporal Masking. In this experiment, we remove the modality and temporal masking for the student encoder during pretraining. This modification results in a slight increase in segmentation performance by $+0.4$ mIoU but a decrease in classification performance by -0.6 F1 score. These ambiguous results are similar to the effects we observed with naive patch dropping. An advantage of including modality and temporal masking is that it reduces the memory requirements during training by up to 30%. Since our goal is to train a single model on several datasets aimed to be fine-tuned for multiple tasks, we keep a unique configuration and adopt this masking strategy.

C. Implementation Details

GeoPlex. See Tab. B for more details on the composition of GeoPlex. GeoPlex is composed of five distinct datasets—TSAT-TS, PASTIS-HD, FLAIR, PLANTED, and S2NAIP-URBAN—which collectively offer a rich combination of data types, including images, time series, and various modalities. These datasets span extensive geographical areas, ranging from 180 km^2 to over $211,000 \text{ km}^2$, and provide a wide array of spatial resolutions (from 0.2m to 250m), temporal resolutions (from 1 to 140 time steps), and spectral resolutions (from 3 to 10 bands). The inclusion of multiple satellite and aerial platforms, such as Sentinel-1/2, Landsat 7/8/9, SPOT6/7, and NAIP, ensures a robust and varied training set.

Network Architecture. AnySat’s architecture follows the Vision Transformer (ViT) template and has 125M learnable parameters, of which 73.6% are modality-agnostic and resolution-adaptive. The components of the model are:

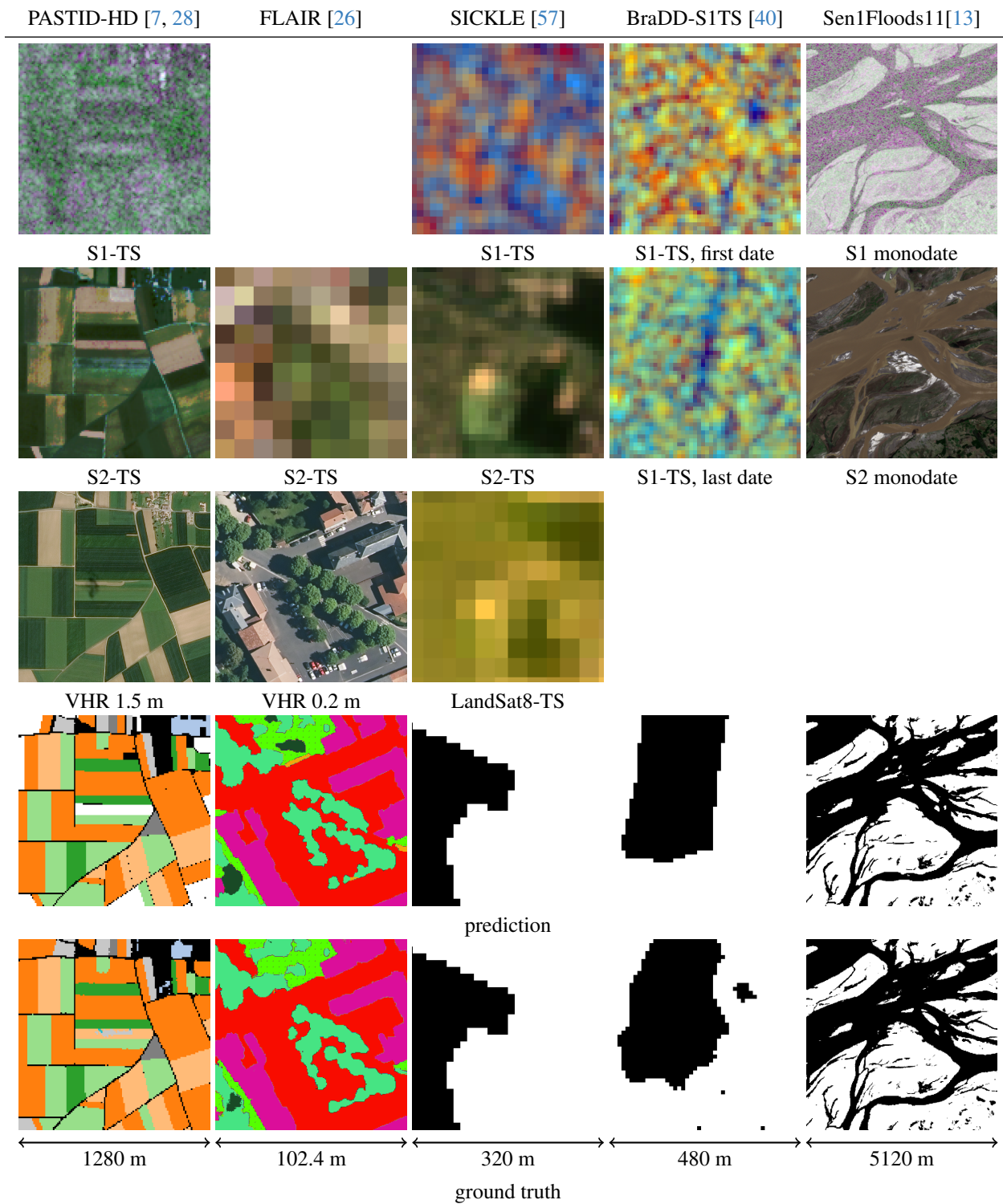

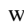











Figure B. **Illustration of Results.** We represent the inputs, predictions, and ground truth for tiles from four datasets. The colormaps are taken directly from the papers. TS: time series, a single date has been chosen. S1/2 stands for Sentinel-1/2. For PASTIS-HD, white parcels are not annotated (void label).

Table A. **Model Performance on the Test Sets of GeoPlex.** For time series, we denote by  when a single date has been selected, and  when seasonal medians have been concatenated in the channel dimension. AL stands for ALOS-2 and MO for MODIS. LP stands for linear probing

Model	Pre-training	Modalities					
TSAI-TS - multilabel classif.		VHR	S1	S2	wF1		
AnySat (ours)	GeoPlex	✓	✓	✓	75.1		
AnySat (ours)	None	✓	✓	✓	72.7		
OmniSat [7]	TSAI-TS	✓	✓	✓	74.2		
DOFA [75]	DOFA	✓			71.6		
PSE+LTAE [27]	None		✓	✓	71.2		
PSE + ResNet [7]	None	✓			68.1		
ScaleMAE [54]	TSAI	✓			62.5		
SatMAE [19]	TSAI	✓			61.5		
CROMA [24]	TSAI	✓			61.0		
UT&T [26]	ImageNet	✓	✓	✓	56.7		
MOSAIXS[55]	TSAI				56.0		
PRESTO [66]	PRESTO				46.3		
Model	Pre-training	Modalities					
PLANTED - classif.		S1	S2	LS	AL	MO	maF1
AnySat (ours)	GeoPlex	✓	✓	✓	✓	✓	61.5
AnySat (ours)	None	✓	✓	✓	✓	✓	61.2
ViViT [5, 53]	None	✓	✓				62.2
ViViT [5, 53]	None	✓	✓	✓	✓	✓	59.3
FLAIR - semantic seg		VHR		S2			mIoU
AnySat (ours)	GeoPlex	✓		✓			55.1
AnySat (ours)	None	✓		✓			55.6
UT&T [26]	ImageNet	✓		✓			56.9
UNet [33]	ImageNet	✓					54.7
UTAE [28]	None			✓			36.1






PASTIS-HD - multilabel classif.		VHR	S1	S2	maF1	
AnySat (ours)	GeoPlex	✓	✓	✓	72.8	
AnySat (ours)	None	✓	✓	✓	65.5	
OmniSat [7]	PASTIS-HD	✓	✓	✓	69.9	
CROMA [24]	PASTIS-HD				60.1	
DOFA [75]	DOFA	✓			55.7	
UT&T [26]	ImageNet	✓	✓	✓	53.5	
UTAE [28]	None		✓	✓	46.9	
ScaleMAE [54]	PASTIS-HD	✓			42.2	
PASTIS-HD - semantic seg		VHR	S1	S2	OA	mIoU
AnySat (ours)	GeoPlex	✓	✓	✓	85.0	66.5
AnySat (ours)	None	✓	✓	✓	84.8	66.3
SkySense [32]	SkySense	✓	✓	✓	85.9	-
UTAE-MM [29]	None		✓	✓	84.2	66.3
TSViT [65]	None			✓	83.4	65.4
UTAE [28]	None			✓	-	63.1
PASTIS-HD - semseg LP		VHR	S1	S2	mIoU	
AnySat LP (ours)	GeoPlex	✓	✓	✓	42.7	
S12-DINO LP [52, 62]	foundation	✓	✓	✓	36.2	
S12-MoCo LP [34, 62]	foundation	✓	✓	✓	34.5	
S12-D2V LP [10, 62]	foundation	✓	✓	✓	34.3	
SpectralGPT [36]	foundation	✓	✓	✓	35.4	
Prithvi [39]	foundation	✓	✓	✓	33.9	

Table B. **Considered Datasets.** We present the detailed composition of GeoPlex, the collection of datasets used for self-supervised training, and our external evaluation datasets.

img: img, **t.s.:** time series: t.s. S1/2: Sentinel-1/2. † upsampled from original acquisition resolution.

Dataset	Extent	Sample Size (S) Patch Size (P)	Modalities	Resolution		
				Spatial (R)	Temporal (T)	Spectral (C)
GeoPlex						
TSAI-TS [3, 7]	50k × (1 img + 2 t.s.) 180 km ² - 4.7 GPix	S = 60m P ∈ {10, 20, 30}m	Aerial VHR	0.20m	1	4
			S1	10m	10-70	3
			S2	10m	10-70	10
PASTIS-HD [7, 28]	2433 × (1 img + 2 t.s.) 3986 km ² - 7.5 GPix	S = 1280m P ∈ {40, 80, 160}m	SPOT6/7	1m [†]	1	4
			S1	10m	140	3
			S2	10m	38-61	10
FLAIR [26]	78k × (1 img + 1 t.s.) 815 km ² - 24 GPix	S = 102.4m P ∈ {10, 20, 50}m	Aerial VHR	0.2m	1	5
			S2	10m	20-114	10
Planted [53]	1.3M × (5 t.s.) 33,120 km ² - 3.0 GPix	S = 120m P ∈ {30, 60}m	S2	10m	8	10
			S1	10m	8	3
			Landsat 7	30m	20	3
			ALOS-2	30m	4	3
			MODIS	250m	60	7
S2NAIP- URBAN [4, 73]	515k × (1 img + 3 t.s.) 211,063 km ² - 136 GPix	S = 640m P ∈ {40, 80, 160}m	NAIP	1.25m	1	4
			S2	10m	16-32	10
			S1	10m	2-8	3
			Landsat 8/9	10m [†]	4	8
External datasets						
BraDD-S1TS [40]	13k × (1 t.s.) 2,995 km ² - 1.2 GPix	S = 480m P = 10 m	S1	10m	20-66	10
Sickle [57]	35k × (2 t.s.) 3,584 km ² - 3.6 GPix	S = 320m P = 10m	S2 Landsat 8/9	10m 10m [†]	13-148 8-34	10 8
TimeSen2Crop [72]	1.2M × (1 t.s.) 120 km ² - 35 MPix	S = 10m P = 10m	S2	10m	29	10
Sen1floods11 [13]	4.8k × (2 img) 125,829 km ² - 2.6 GPix	S = 5120m P = 80m	S2	10m	1	10
			S1	10m	1	3

- **Modality Projectors ϕ_m^{proj} (33M parameters for 11 projectors).** These modules are MLPs responsible for projecting the input data of each modality into a common feature space.
- **Spatial Transformer ϕ^{trans} (45M parameters).** Composed of three self-attention transformer blocks, this module captures the spatial relationships between sub-patches for each modality and patch.
- **Modality Combiner ϕ^{comb} (49M parameters).** This module consists of three self-attention blocks followed by a cross-attention block, and merges the representations from different modalities into a unified feature vector for each patch.
- **Predictor ϕ^{pred} (29M parameters).** Exclusive to the student, this module is a single self-attention block and predicts the teacher’s embeddings for the dropped patches.

Handling MODIS data. In the Planted dataset [53], MODIS observations are included, but their resolution (250 meters) is larger than the entire observed tile (120 meters). We treat these observations as *context* tokens: we concatenate their ϕ^{patch} embeddings to the $|\mathbf{M}| \cdot (S/P)^2$ tokens from all other modalities. We do not add positional encoding, and this token is not included in the contrastive loss.

Optimization Parameters. To better manage our memory usage, we adapt the batch size to the size of the samples of each dataset: TreesatAI-TD: 384, PASTIS-HD: 8, FLAIR: 96, PLANTED: 2048, S2NAIP: 16. We use 8 NVIDIA H100 for experiments on GeoPlex, PLANTED and Pastis-HD, and

a smaller cluster of 3 A600 for TreeSatAI-TS and FLAIR.

Beyond the changes above, all optimization parameters are shared across all datasets. We used the AdamW [43] optimizer with a learning rate of 5×10^{-5} for all our experiments (pretraining and fine-tuning). We used a LinearWarmupCosineAnnealingLR [1] for classification and ReduceLROnPlateau [2] scheduler for pretraining and segmentation.

We set the contrastive temperature γ to 0.1 to n Eq. X. We used an EMA decay of 0.996. All other hyperparameters are shared with [original JEPA implementation](#).

Position Encodings. We describe here our scale-adaptive positional encoding which allows us to use the same encoders for different resolutions, scales, and patch size. The input tokens to the modality combiner ϕ^{comb} correspond to patches of size $P \times P$ meters, while those to the spatial transformer ϕ^{trans} represent subpatches of size $(R_m \delta_m) \times (R_m \delta_m)$ meters. Here, R_m varies per sensor modality m , and P is randomly chosen for each batch during training. To train a single scale-aware model capable of handling varying resolutions, we employ a scale-adaptive positional encoding inspired by Scale-MAE [54].

We use the same positional encodings in ϕ^{comb} and ϕ^{trans} . We first describe the positional encoding of a token by ϕ^{comb} . We denote by pos_x the index of the token’s patch within its tile along the x -axis; similarly, pos_y along the y -axis. If the embeddings of the token have a dimension D , the positional encodings $\mu_x(\text{pos}_x, i)$ and equivalently $\mu_y(\text{pos}_y, i)$ are of size $D/2$. For $i \in [0, D/2[$ we have:

$$\mu_x(\text{pos}_x, i) = \sin \left(\frac{g}{G} \frac{\text{pos}_x}{10000^{\frac{i}{E}}} + \frac{\pi}{2} \text{mod}(i, 2) \right), \quad (\text{A})$$

where $g = P$ is the size in meter of the patch considered unit: patch of size for ϕ^{comb} , and G is a reference length that we set to one meter. We compute $\mu_y(\text{pos}_y, i)$ similarly, and the positional encoding is the channelwise concatenation of both vectors. The positional encoding is directly added to the embeddings.

For ϕ^{trans} , we define the positional encoding of each subpatch within its patch with the same formula, but set g to $g = R_m \delta_m$, the size of the subpatch in meter.

D. Datasets and Tasks

Here, we provide more details about the datasets used to train and evaluate AnySat and their associated tasks. See Tab. B for an overview of the datasets used in GeoPlex.

TreeSatAI-TS [3, 7]: This multimodal dataset is designed for tree species identification and consists of 50,381 tiles,

each covering an area of 60×60 meters, with multi-label annotations across 20 classes. All data were collected in Germany. The dataset includes Very High Resolution (VHR) images at 0.2 m with a NIR band, Sentinel-2 time series, and Sentinel-1 time series.

PASTIS-HD [7, 29]: This crop mapping dataset supports classification, semantic segmentation, and panoptic segmentation. Each agricultural parcel is delineated at a resolution of 10 m and annotated across 18 crop types. The dataset contains 2,433 tiles with an extent of $1,280 \times 1,280$ m, including Sentinel-2 time series, Sentinel-1 time series (we use only the ascending orbit), and SPOT6 VHR imagery at 1.5 m resolution.

FLAIR [26]: This dataset combines VHR aerial imagery at a 0.2 m resolution with Sentinel-2 time series data and comprises 77,762 tiles acquired across metropolitan France. The VHR images include five channels: RGB, near-infrared, and a normalized digital surface model derived by photogrammetry. Each VHR pixel is annotated with one of 13 land cover classes.

PLANTED [53]: The PLANTED dataset is specifically designed for tree species identification and features 1,346,662 tiles of planted forest across the world. Each tile is associated with one of 40 distinct classes. This dataset integrates imagery from five different satellites with various resolutions: Sentinel-2 (10 m), Landsat-7 (30 m), MODIS (250 m), as well as radar time series from Sentinel-1 (10 m) and ALOS-2 (30 m). The time series are temporally aggregated at various intervals—seasonally, monthly, or yearly.

S2Naip-Urban [4, 73]: This dataset includes images captured at the same locations as the S2NAIP-Urban super-resolution dataset [73], which is a subset of the extensive S2NAIP [4] dataset focused on urban areas. This split comprises 515,270 tiles, featuring imagery from NAIP at a 1.25 m resolution, Sentinel-2 and Sentinel-1 time series, and Landsat-8/9 data rescaled to a 10 m resolution. We use this dataset for pretraining only because there are no official labels and evaluations.

BraDD-S1TS [40]: BraDD-S1TS (Brazilian Deforestation Detection) is a change detection dataset comprising Sentinel-1 time series of the Amazon rainforest, aiming to segment deforested areas. It includes 13,234 tiles covering regions with varying deforestation rates, providing pixel-wise binary annotations for deforestation events occurring between the time series’ first and last radar image.

Sickle [57]: SICKLE is a multimodal crop mapping dataset from India containing 34,848 tiles with Sentinel-1, Sentinel-2, and Landsat-8 time series. We use the paddy / non-paddy culture binary semantic segmentation task. As the test set has not been released by the authors, we perform our experiments on the validation set.

TimeSen2Crop [72]: TimeSen2Crop is a crop mapping dataset consisting of 1,212,224 single-pixel Sentinel-2 time series, a configuration not present in GeoPlex. It includes

data from Slovenia with annotations for 16 different crop types.

Sen1floods11 [13]: Sen1Floods11 is a flood segmentation dataset featuring 4,831 pairs of Sentinel-1 and Sentinel-2 images, each annotated with dense flooded/not-flooded labels. The dataset spans diverse global regions, with each tile covering a 5120×5120 m area (2600 hectares) and containing a single acquisition date per sensor.